COBEM 2023 27TH INTERNATIONAL CONGRESS OF MECHANICAL ENGENEERING

ABCM Brazilian Society of Mechanical Sciences and Engineering
27th ABCM International Congress of Mechanical Engineering
December 04-08, 2023, Florianópolis-SC, Brazil

COB-2023-0191
PRELIMINARY STUDY OF A SPACE MISSION FOR OBSERVING PLASMA BUBBLES IN THE IONOSPHERE USING GNSS-RO

Vinicius Fernandes
Rogério Pirk
Willer Gomes Santos
Instituto Tecnológico de Aeronáutica
vinicius.vfernandes@ga.ita.br
rogeriorp@fab.mil.br
willer@ita.br

Abstract. *Equatorial plasma bubbles (EPB) result from the interaction of solar winds, twilight, ionosphere, and Earth's magnetosphere. Understanding these phenomena is crucial for developing radio communication systems that interact with the ionosphere. Global Navigation Satellite System Radio Occultation (GNSS-RO) technology has been employed to study EPB. This work aims to conduct a preliminary study of a mission using the ARCADIA method for model-based system engineering and methodology of space mission analysis and design. The primary mission objective is to observe EPB using GNSS-RO. Mission requirements were derived from radio occultation physics and operational stakeholders. The mission architecture proposed is a minimum constellation of three satellites in circular orbits, with an apogee of 7400 km, inclination of 51.64°, and varying ascending nodes at 10° intervals to form an occultation zone for GNSS signal interception. The scientific payload comprises a radio receiver, a GNSS signal processing computer, a UHF/VHF/X-band ground signal receiver-transmitter, an onboard mission clock, and a control computer. Estimated budgets include electrical power (152.4 W), mass (5.02 kg), operational temperature range (30°C to 50°C), and satellite dimensions (4U). The chosen propulsion system is the polytetrafluoroethylene (PTFE) plasma propulsion, providing a velocity increment of 613.25 m/s.*

Keywords: *ionosphere, satellites, GNSS-RO, SMAD, MBSE*

1. INTRODUCTION

The investigation of equatorial ionospheric plasma bubble formation, referred to as ionospheric equatorial plasma bubbles (EPB), gained significant attention since the early 2000s with several space missions focused on studying this phenomenon. Theoretical investigations have primarily involved physicists and climatologists, associating their formation with external events such as gravitational waves, solar winds, and Earth's magnetosphere (Dos Santos Prol et al., 2018). Recent studies indicate that the interaction between the ionospheric F region and the equatorial solar penumbra zone acts as an initiator of EPB formation (Takahashi et al., 2018). EPB can significantly impact the local electron concentration in the ionosphere, leading to diffraction effects on electromagnetic signals passing through the bubbles, thereby introducing oscillations and noise into the communication channel (Moraes et al., 2018).

The study of EPB has extensively employed the radio occultation technique, utilizing satellite constellations. Notably, the Constellation Observing System for Meteorology, Ionosphere, and Climate (COSMIC) mission stands as a successful example with substantial results (Kepkar et al., 2020). In this mission, the diffraction of signals from the Global Navigation Satellite System (GNSS) traversing the Earth's atmosphere to measure climatic parameters, and provided data for calculating electron density in the atmosphere, revealing the presence of EPB.

This study presented a proposal for the development of a space mission aimed at observing the formation of EPB in the equatorial region. The work employs the GNSS-RO technique and was designed around a minimum constellation of three satellites. To accomplish this objective, conceptual project methodologies and systems engineering techniques were implemented. The primary goal was to evaluate the suitability and effectiveness of the Space Mission Analysis and Design (SMAD) method (Larson et al., 1997), complemented by the model-based system engineering methodology (Bussemaker et al., 2022).

2. METHODOLOGY FOR THE SPACE MISSION PROPOSAL DEVELOPMENT

The development of this mission, aimed at observing the formation of EPB, was systematically divided into operational and non-operational assessments. The operational portion involved evaluating the technical aspects of the mission, including orbit design, payload specifications, onboard equipment, and other pertinent considerations from the fields of aerospace, mechanical, and electrical engineering. Conversely, the non-operational assessment encompassed the

examination of stakeholders' interests, the harmonization of operational requirements and constraints, concurrent engineering practices, and mission planning.

The workflow employed for the establishment of the operational portion was the Space Mission Analysis and Design (SMAD). This methodology starts with the identification of one or more high-level objectives and constraints for a space mission, progressing to the definition of a space system that can achieve these overarching objectives while minimizing costs. Furthermore, the SMAD process starts with the assessment of stakeholders and mission objectives, and then proceeds through the comprehensive technical evaluation of the proposed architecture using performance and merit figures. The ultimate aim is to deliver the preliminary mission design, which includes mission objectives, operational orbit, and first iteration of satellite design proposal (Larson et al., 1997).

The non-operational portion was addressed using ARCADIA-Capella-MBSE® (Voirin, 2017). In Phase A of SMAD, the mission's structural proposal, stakeholders, interactions between operational players, and the scientific payload proposition were defined.

2.1 Definition of Mission Objectives

The main objective of this space mission is to serve as an observation instrument for detect and measure EPB in the Earth's ionosphere. To achieve successful observations and valid data, this project must be capable of detecting and geolocating the referred EPB. The adopted scientific and technological testing technique is GNSS-RO (Yue et al., 2014). In order to fulfill the main objective, the mission must establish communication links with the GNSS constellation as well as ground communication stations (GCS) for mission control and data exchange. The geolocation of the EPB will be accomplished through data processing, conducted by the mission's research and development team.

As a technological demonstration or study platform, the capability for formation flight has been proposed, which generates the operational requirement of a satellite constellation or formation flying. The relationship is shown in Figure 2.

Figure 1 illustrates the hierarchical relationships among missions, capabilities, and key stakeholders, stemming from the mission's main objective, or, mission statement. Fulfilling the set of project requirements ensures mission compliance and clarifies the link from between stakeholders and their interests. The entity M represents the guiding mission, and the entities C are proposed capabilities to fulfill the mission. The relationships <<e>> indicate the extension of one capability to another, and <<i>> indicate the inclusion of capabilities in a larger one. The entity **SA** stands for system actor, representing that once the actor is related to the mission or capability, there's some degree of responsibility of the actor into the planning, execution, funding, or any other interaction needed for the mission success.

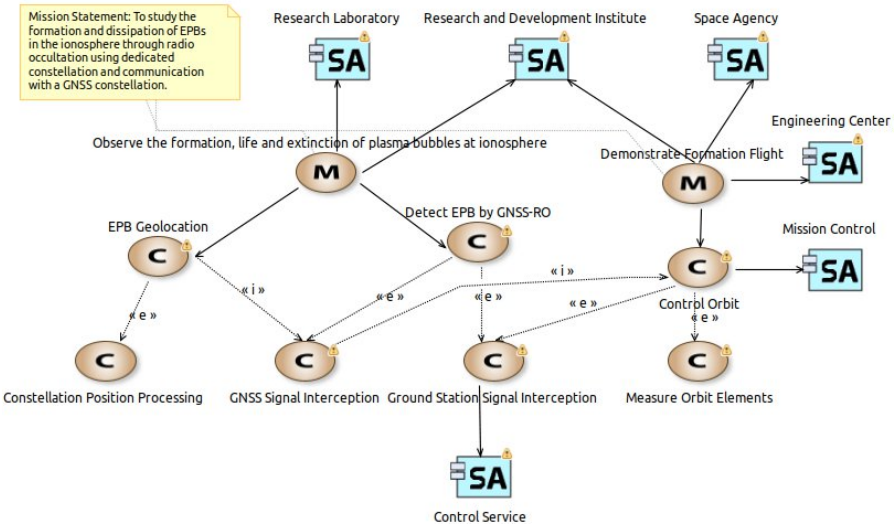

Figure 1. Mission capability diagram – MCD - of the scientific objective of the mission related to EPB, and engineering objective related to flight formation.

2.2 Stakeholders listing

The list of stakeholders interested in the mission was created considering separate operational entities with distinct roles, such as the contractor, developer, builder, and mission operator. This division, indicates the operational actors that interact with the mission, which the importance to the analysis lies in the capacity of listing all the requirements each operational entity imposes to the mission, and the shared responsibility.

The stakeholders are defined as: space agency, launch contractor, research and development institute, research laboratory, engineering center, builder, control service, mission control, and telecom and telemetry center.

2.3 Operational and non-operational requirements

The requirements and design constraints were identified based on constraints originating from operational entities. These requirements interact with the mission's capabilities, imposing constraints on the design. Such constraints influence the orbit design, launch strategy and control components.

In this framework, the ARCADIA meta model emerges as a formal reconcile between the requirements and desires of operational entities, incorporating quantitative aspects and design decisions. The same relationship is depicted in Figure 2, illustrating the reconciliation of the constraints imposed by the engineering team with the capabilities related to the missions.

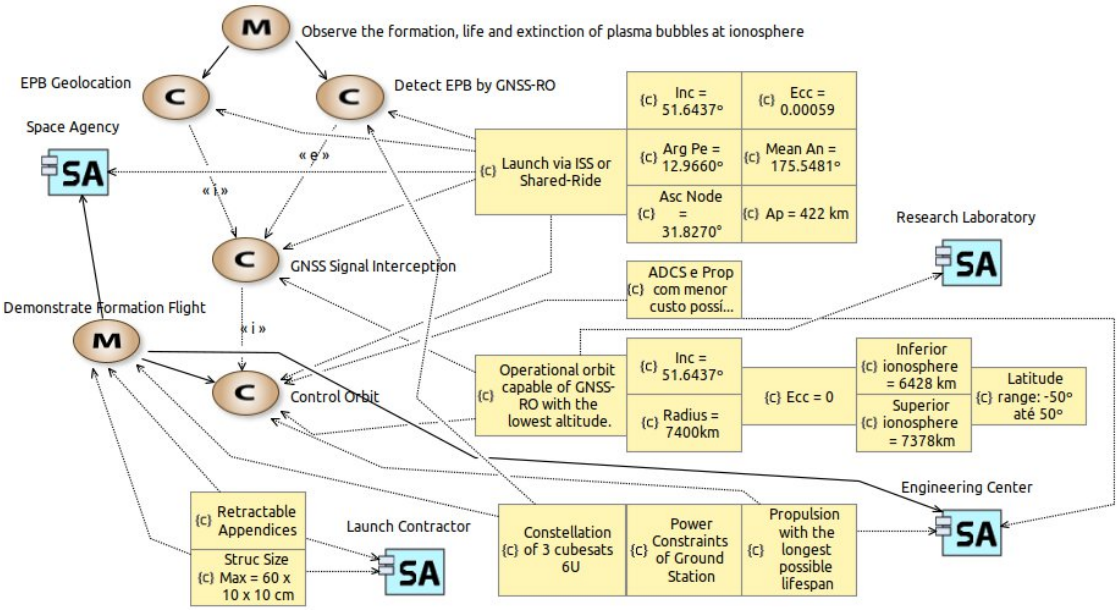

Figure 2. MCD of the operational constraints – yellow boxes - and requirements associated with the mission and capabilities – **M** and **C** entities respectively - and its respective proposer system actors – **SA** entities.

The operational orbit constraints are derived from the probability distribution of EPB formation, as demonstrated by Sidorova, 2020. This probability distribution extends across the entire ionospheric range, from an altitude of 300 km up to 1600 km, with a latitudinal spread ranging from -60º to 60º. Therefore, positioning a satellite in the upper range, between 1000 km and 1600 km, enhances the variability of EPB observations by expanding the vertical range of possible radio occultation, while maintaining latitudinal coverage.

The requirements for the operational orbit were determined considering the minimum possible variation in velocity (ΔV) between the launch orbit from the international space station (ISS) and the operational orbit, in order to minimize costs. The orbital inclination of 51.64º ensures latitudinal coverage from -50º to 50º, eliminating the need for orbital plane changes.

The orbital radius was calculated from geometric relationships for radio occultation, simplified from Zou (2020). The impact parameter **a**, here defined as the vector from the center of mass of Earth to the asymptote of the GNSS signal refraction point, shown in Figure 3, was constrained within the ionosphere radius range, depicted as the blue belt at Figure 3, which correspond to the range of interest for EPB observations for this mission. The red line represents the GNSS signal traversing the atmosphere, the impact parameter **a**, the refraction angle α, and the orbital radius $\mathbf{r_G}$ and $\mathbf{r_L}$ for the Global Positioning System (GPS) satellite and GNSS-RO satellite respectively, and ϕ_G and ϕ_L as the GNSS signal angle patch for the GPS emission to the GNSS-RO satellite reception.

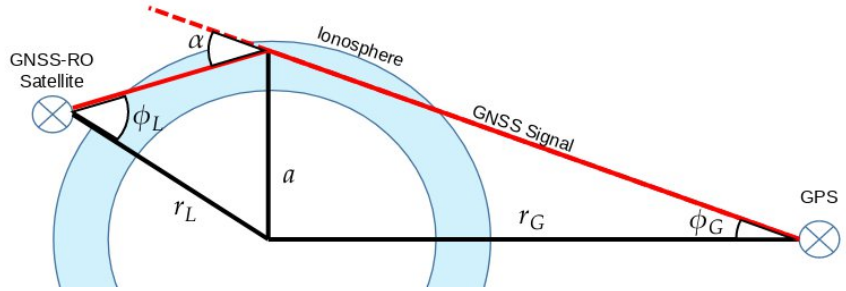

Figure 3. A diagram illustrating the geometric parameters of radio occultation.

The geometric relationships of radio occultation are presented in Equations (1) and (2), where solutions for the refraction angle α are obtained only when the orbital radius $\mathbf{r_L}$ of the satellite in low Earth orbit is larger than the impact parameter **a**, assuming an ideal atmosphere without refraction disturbances.

$$a = r_L \sin\phi_L, \tag{1}$$

$$\alpha = \phi_G + \phi_L + \arccos\left(\frac{r_G r_L}{r_G r_L}\right), \tag{2}$$

3. MISSION PROPOSAL AND FIRST APPROXIMATIONS

A generic satellite design has two main subsystems: the bus platform, used as the supporting system and overall physical structure, and the payload, which is mounted to the bus and executes the satellite capabilities. The overall satellite can be defined as the system of the following subsystems: power generation, propulsion, attitude determination and control, thermal control, environmental control, and telemetry, tracking and command, as proposed by dos Santos, (2009), for the preliminary study of Equatorial Atmosphere Research Satellite (EQUARS). This study adapts this approach for a satellite composed of the following subsystems: mission payload, attitude determination and control, propulsion, communications, power generation, thermal control, and CubeSat bus.

3.1 Mission payload design and proposal

The conceptual design of the payload was carried out by listing the logical functions and allocation into physical components.

The logical functions provide detailed algorithms that need to be executed to achieve the associated capability. In this analysis, it was chosen to group the logical functions into functional chains of larger tasks, as depicted in Figure 4. The blue lines represent the executed GNSS-RO function chains, and the red lines represent mission control functional chains. Both chains are executed on the satellite, with all functions painted blue. The green functions are executed by other system actors, not defined in the physical architecture in this study. RINEX stands for receiver independent exchange format, used in satellite navigation.

The logical functions are then allocated to behavioral functions, which group these functions associated with subsystem components, fully characterizing the physical component with its expected behavior, its logical function in the system, and its physical connections and exchanges.

The difference between logical functions and system functions lies in their semantics. System functions are arbitrary tasks associated with entities and subsystems, while logical functions are algorithms that can be associated with operational actors and system components.

This characterization completes the conceptual design of the scientific payload for the EPB determination mission, shown in physical function architecture breakdown diagram – PFABD - in Figure 5. The necessary components then are: GPS antenna, ground communication antenna, dedicated GNSS signal processing onboard computer, and mission control onboard computer. The electrical and structural components are common to other subsystems. The green lines represent logical exchanges between functions, while the blue lines represent physical exchanges or paths that facilitate the logical exchanges. The yellow lines represent physical connections between the components.

3.2 Operational orbit and perturbation analysis

A circular operational orbit is proposed, with variation in the orbital plane for each one of the three satellites in the constellation. The orbital radius value comes from the solution of the refraction model presented at Equations (1) and (2) considering the ionosphere radius range from 6428 km to 7378 km as the impact parameter and the GPS orbit radius of 26578 km, resulting in a minimum orbital radius of 7400 km for refraction angles of 0.30º to 27.70º. Considering that for EPB observation by GNSS-RO technique the GPS signal must traverse the target region and suffer interference by the

EPB formation (Kepkar, 2020), this orbit was accepted as favorable first approach to the analysis of the total cost for the operational orbit launch, described as ΔV in Table 1, and serves as input for the upcoming disturbance, propulsion, telecommunications, and thermal dissipation analysis. The elements of the operational orbit are described in Table 2.

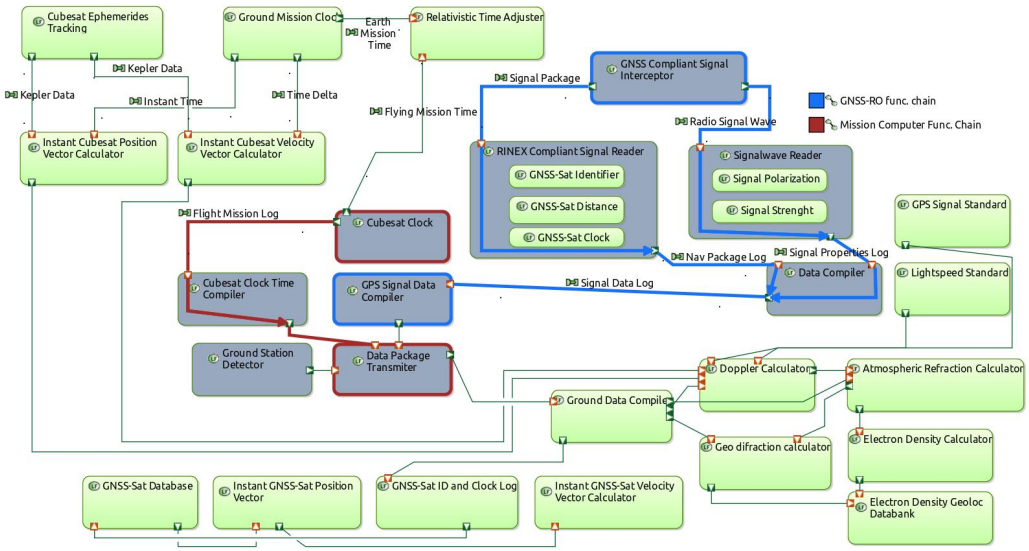

Figure 4. Logical architecture breakdown diagram – LABD - of the logical functions that must be performed to achieve the mission capability of EPB detection via radio occultation.

The orbital planes and occultation zone are shown in Figure 6. Note that the variation in the longitude of the ascending node creates the separation of the orbital planes, and the variation in mean anomaly creates a positional offset in the orbit, resulting in a triangular formation flying.

The proposed formation flying achieved the largest occultation zone area in the equatorial region, with 1.29×10^6 km², and the smallest area recorded at latitudes of 50º, with 4.97×10^4 km². The variation between the smallest and largest obtained occultation zones was 96%, with the largest variation in satellite-to-satellite distance between 1 and 2 ($\mathbf{r}_{L12}$) being 12%, and between satellite 1 and 3 ($\mathbf{r}_{L13}$) being 38%, with the highest distance at 2300 km mark, and lowest at 1600 km mark. Since this study is conceptual and preliminary, no active control model for the occultation zone size and distance is proposed.

The occultation zone area A_{il} was calculated using the vector model shown in Equations (3) and (4), with the satellite coordinates projected onto the J2000 equatorial coordinate system based on orthogonal vector projection from body i to l ($\mathbf{r}_i$ - $\mathbf{r}_l$).

$$\left(r_{ix} - r_{lx}\right) + \left(r_{iy} - r_{ly}\right) + \left(r_{iz} - r_{lz}\right) = r_{li}, \tag{3}$$

$$\| r_{12} \mathbf{x}\ r_{13} \| = A_{il} \tag{4}$$

The torque disturbances to which the satellites are subjected, due to magnetic, gravitational, aerodynamic, and solar radiation disturbances, were calculated based on velocity data, atmospheric density, altitude, and latitude of a probing orbit with a perigee altitude of 400 km, apogee altitude of 1022 km, and inclination of 51°. The parameters obtained from the disturbance calculations are described in Table 3 for the equations recommended by SMAD, considering the pressure center and solar pressure center at the geometric 4U CubeSat's center. The length counts with the solar panel surface needed for power generation fully deployed (Larson, 1997).

The disturbance propagation was simulated using NASA's GMAT propagator PrinceDormand78 with step0, with JacchiaRoberts atmospheric model. The drag coefficient and surface reflectivity are general recommendations for disturbance simulation in CubeSats (Kilic et al., 2013).

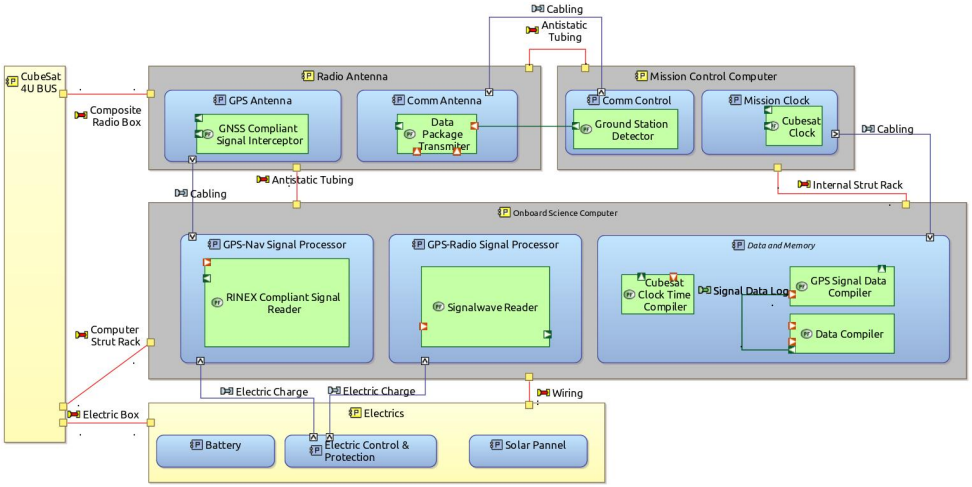

Figure 5. PFABD of the proposed payload, depicting the logical functions allocated to expected behavioral functions (blue) of associated physical components (yellow for not payload related and gray for payload component).

Table 1. Journey to the operational orbit and ΔV costs.

Journey step	ΔV **(m/s)**
1 – ISS launch	2.00
2 - ISS drift (one complete drifting orbit)	0.00
3 – Orbit transfer burn	160.1
4 – Orbit circularization burn	158.9
5 – Operational orbit maintenance	50.00
6 – Deorbit burn	242.20
Total cost (m/s)	**613.25**

Table 2. Operational orbit and variation of the longitude of ascending node – LNA – and mean anomaly between the three satellites.

Circular orbit radius (km)	7400
LNA variation	0º; 10º; 20º
Apogee velocity (km/s)	7.33
Altitude (km)	1022
Variation of mean anomaly	0º, 10º, 20º

The largest torque value found, composed of the sum of all disturbances, was 22.493 μNm, with the magnetic torque contributing 80% of the total value. The contribution of the other torques sums up to 20% of the calculated total, with a total variation between perigee and apogee of 47%. The behavior of torque variations related to the composition of all disturbances is presented in Figure 7.

Due to the low atmospheric drag value found, the calculated orbit decay time is estimated to over 40 years considering previous study from Vries (2010), which considered the value of 2.3 as drag coefficient for CubeSats, used in this study.

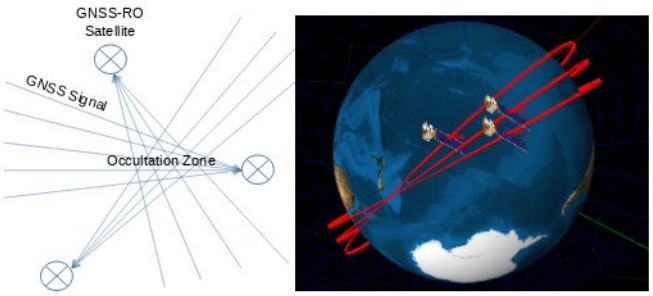

Figure 6. Proposed flight formation with variation of the orbital plane through changes in the longitude of the ascending node and mean anomaly. This variation allows for an occultation zone with maximum area at the equator.

Table 3. Design parameters for disturbance calculation.

Center of mass	0	Drag coefficient	2.3
Aerodynamic pressure center	0.5	Iz=Id	0.008
Magnetic dipole	1	Iy=Ih	3.111
Total Mass (kg)	5.17	Total area (m²)	0.80128
Lenght (m)	2.69	Solar pressure center	0.5
Height (m)	0.1	Surface reflectivity	0.6

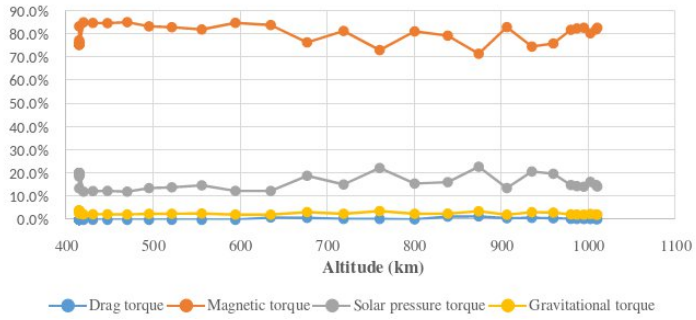

Figure 7. Variations of disturbance torques as a function of satellite altitude.

3.3 Attitude determination and control

Attitude determination was designed to utilize data from a magnetometer, combined with a coarse solar sensor embedded at the EXA's deployable multifunction solar array (DMSA) solar panels (DMSA, 2023). Attitude control was designed to use reaction wheels and magnetic actuators, for reaction wheels desaturation. An integrated control unit was chosen, incorporating attitude magnetic sensor, reaction wheels, and magnetic actuators, to reduce project development costs and meet the requirement of minimizing attitude control expenses. Mass and force data required for attitude control, based on the maximum magnetic disturbance torque, are provided in Table 4. The data was calculated using the SMAD equation table (Larson, 1997). The pointing error requirement considered was 5 degrees.

Table 4. Parameters of the integrated attitude control system.

Reaction wheel radius (m)	0,04
Angular velocity (RPM)	2000
Angular momentum for actuation (Nms)	0,04
Reaction wheel mass (kg)	0,26
Magnetic dipole for actuation (Am^2)	1.07 Am^2

3.4 Propulsion

The main challenge in propulsion was to find a lightweight and compact technology that could meet the mission's ΔV cost without adding complexity to the design, and be safe for a launch from the ISS. A trade-off study, shown in Table 5, was conducted among commercial solutions, with PTFE plasma electric propulsion technology showing the best fit for the listed requirements in Table 5 (Woodruff, 2022). The amount of propellant required was calculated using Tsiolkovsky's equation (TSIOLKOVSKY, 1911).

Table 5. Trade-off study among researched propulsion solutions.

	Cold gas	Arc jet	Hall thruster with noble gas	PTFE Plasma	Liquid bi-propellant
Multiple firing capacity	OK	OK	OK	OK	OK
Quick firing – no need of previous heating	OK	OK	OK	OK	OK

Non-toxic propellant	OK	NOT OK	OK	OK	NOT OK
Needed propellant (kg)	5.00	3.20	0.3	1.13	4.4
Thrust (N)	1.00	0.0150	0.0025	0.0034	0.5000
Specific impulse (s)	40.0	600.0	8500.0	2400.0	285.0
Energy budget (W)		1000	60	48	12
Mass budget (kg)	20	1.6	3.1	1.9	3.0

3.5 Communications

Two antennas were calculated for VHF uplink for control and UHF downlink for tracking, and XBand downlink for data transmission needs, considering as benchmark the Scintillation Prediction Observation Research Task (SPORT) and the Brazilian National Insitute for Space Research (INPE) telemetry, tracking and control (TT&C) ground stations and nanosatellites development recommendations (Gomes, 2021, Orduy, 2016). The antenna parameters were taken from ISIS and Endurosat commercial solutions (ISIS, 2023, Endurosat, 2023a), as benchmark models for this mission antennas considering to size and components mass. The values of signal-to-noise ratio, digital signal-to-noise ratio, and gain-to-temperature ratio (G/T) were calculated using the SMAD equation table. The calculated values for the onboard antennas are shown in Table 6.

Tracking operations may be done using onboard GPS antennas and signal receiving, considering radio communication failure scenarios, as demonstrated by previous work of Chiaradia (2009).

Table 6.Calculated values for commercial antennas ISIS Deploy Antenna and Endurosat 2x2.

	VHF/UHF COTS Antenna (ISIS Deploy Antenna)		XBand COTS Antenna (Endurosat 2x2 X)
	VHF Uplink	UHF Downlink	Xband Downlink
Frequency range	145 ~ 146 (MHz)	400 ~ 438 (MHz)	8.052 GHz
Antenna efficiency	55%	55%	55%
Peak Gain	0 dB	0 dB	12 dB
Half-Power beamwidth	120º	120º	40º
C/No (Carrier to noise density ratio)	75.33 dB	63 dB	90.57 dB
Eb/No (Energy per bit noise density ratiol)	35.5 dB	23.17 dB	17.56 dB
Margin Eb/No	19.1 dB	9.67 dB	10.16 dB
Probability of Bit Error	1.00E-6	1.00E-6	1.00E-6
Required Eb/No	10.50 Db	10.50 dB	10.50 dB
G/T (Gain to noise temperature ratio)	-33.01 dB/K	-21.00 dB/K	-30.80 dB/K
Mass Budget	0.085 kg		0.0232 kg

3.6 Onboard processing

The need for two onboard computers was considered, one for mission control, with the basic central processing unit (CPU) handling VHF/UHF/XBand antennas, TT&C, and mission memory, while the payload computer takes care of mission clock, dedicated memory, and analog and digital GNSS-RO signal processing.

The chosen computers were the Endurosat OC+GNSS Receiver for GNSS-RO processing at the payload, and the Data Patterns DP-OBC-04902 CPU for mission computer (Endurosat, 2023b, Data Patterns, 2023).

3.7 Mass budgets, thermal control, power, and volume

After selecting commercial solutions for the satellite, the next step is to size the thermal control system, determine the required power, and assess whether the volume needed to accommodate the components is compatible with a CubeSat structure, as well as calculate the final mass of the satellite.

The complete list of selected commercial components, along with their properties, shown in Table 7, serves as input for the mass, thermal control, power, and volume budgets.

The total calculated power requirement is 72 W, with a peak factor of 2.07, resulting in a total energy requirement of 152.4 W. Considering a power density of 260.86 W/kg and an efficiency of 28% for the EXA DMSA panel, the total calculated panel area is 0.68 m², with a total mass of 0.6 kg and a array span of 2.68 m. The efficiency of the commercial UMPPT Solar Panel Joiner converter is 92%, thus delivering 140.2 W, requiring a larger panel area and a different array and panel layout to reach the requirement power (UMPPT, 2023). The batteries were calculated based on an energy density of 246 Wh/kg for a solar eclipse duration of 35 minutes, with a constant supply of 73.5W, resulting in a battery mass of 0.4 kg.

The thermal requirement of the satellite was calculated considering a total area of 0.801 m², including the CubeSat's body and solar panels, with an emissivity of 80% and absorption of 60%. At an altitude of 1022 km, a solar albedo of 0.986 was considered, with an albedo of 34% and a solar flux of 1418 W/m². The maximum planetary emission is 258 W/m², and the dissipation power is 73.5 W. The thermal equilibrium range was calculated to be -44.4ºC to 32.6ºC. If considered the optimal operating range of 30ºC to 50ºC, an internal heater and an additional thermal dissipation area of 0.149 m² are required. The implementation of this additional area and the heater is an open problem.01

The total volume of the CubeSat was calculated by considering the volumes occupied by the subsystems, using a parallelepiped with a face of 99 x 99 mm and a variable length for accommodation. The required length is 253.2 mm, resulting in a 3U CubeSat, but accounting for the accommodation with the structural components and the space for heater accommodation, an additional 1U was added, totaling 4U.

The total mass of the satellite was calculated by adding the mass of all components, propellant, and estimating the structural mass using a density of 0.08 kg/U.

Table 7. List of commercial components considered in the analysis, mass, power, and proposed final volume to accommodate all components.

Payload	Commercial Component	Mass (kg)	Power (W)	Thermal range (ºC)	Volume (mm)
GPS-Receiver	Endurosat OC+GNSS Receiver	0.18	4	-40 ~ 55	99 x 99 x 20
		Propulsion			
Propellant	Solid PTFE	1.13		-10~50	
Engine	CUA FPPT	1.88	48	-40 ~ 80	98 x 98 x 160
		Communications			
VHF/UHF	ISIS Deploy Antenna	0.085	2	-20 ~ 60	98 x 98 x 7
Xband	Endurosat 2X2	0.0232	4	-20 ~ 60	60 x 60 x 7
		Attitude Control			
Magnectic Actuator	Tensor Tech ADC-MTQ (2023a)	0.14	3	-20 ~ 60	98 x 98 x 20
Reaction wheel	Tensor Tech RS100 (2023b)	0.25	1	-20 ~ 60	64 x 64 x 10
CPU	DP-OBC-0402	0.09	3	-40 ~ 55	90 x 99 x 15
		Power			
Solar panel	EXA DMSA	0.6		-40~125	
Batteries	BA01 (EXA, 2023)	0.4		30~80	89 x 95 x 14
Conversor	UMPPT Solar Panel Joiner	0.023		-40~80	90 x 45 x 7.2
		Thermal control			
Heater					1 U
Structure		0.226			2.532 U
	Totals	5.02 Kg	72.0 W	30~50	4 U (proposed)

4. CONCLUSION

The use of ARCADIA-MBSE and SMAD together has proven useful to design and approximate a mission based solely on initial proposals and a desired physical phenomenon to observe.

The proposed mission uses a minimum number of three 4U CubeSats in a 7400 km radius, 51.64° inclination, circular orbit, The orbital plane would vary by changes of 10º in ascending node, resulting in the formation of an occultation zone, enabling GNSS-RO observations. The payload consists of a GPS signal antenna and signal processing computer, a UHF/VHF/Xband ground signal receiver-transmitter, an onboard mission clock, and a control computer. Estimated budgets include electrical power (73.5 W), mass (5.17 kg), operational temperature range (30°C to 50°C), and satellite dimensions (4U). The chosen propulsion system is solid PTFE plasma propulsion, providing a velocity increment of 613.25 m/s.

In this study, a single design loop was performed, which left engineering questions to be defined on posterior studies regarding sensor requirements, thermal control needs, power consumption and dissipation, the feasibility of using PTFE propulsion, the physical structure of the satellite, further customization of the commercial of the shelf (COTS) subsystems, and the control model for a triangle formation flying with different orbital planes.

5. ACKNOWLEDGEMENTS

This study was financed in part by the Coordenação de Aperfeiçoamento de Pessoal de Nível Superior - Brasil (CAPES) - Finance Code 001.

6. REFERENCES

BUSSEMAKER, J. H.; CIAMPA, P. D. MBSE in Architecture Design Space Exploration. Handbook of Model-Based Systems Engineering, p. 1–41, 2022.

CHIARADIA, A. P., et al. Satellite Orbit Determination Using Short Arcs of GPS Data. Applied Mechanics and Materials. Trans Tech Publications, Ltd., December 2014.

DATA PATTERNS On Board Computer DP-OBC-0402 | Satsearch. n.d. Satsearch.co. Accessed July 9, 2023. https://satsearch.co/products/data-patterns-on-board-computer-dp-obc-0402.

DMSA Micro: Deployable Multifunction Solar Array with Embedded Antennas, Magnetorquers, and Sensors | Satsearch. n.d. Satsearch.co. Accessed July 9, 2023. https://satsearch.co/products/exa-dmsa-micro-deployable-multifunction-solar-array-with-embedded-antennas-magnetorquers-and-sensors.

DOS SANTOS PROL, F. et al. Tomographic Imaging of Ionospheric Plasma Bubbles Based on GNSS and Radio Occultation Measurements. Remote Sensing, v. 10, n. 10, p. 1529, 23 set. 2018.

DOS SANTOS, W.A. et al. A Knowledge-Based and Model-Driven Requirements Engineering Approach to Conceptual Satellite Design. In: Laender, A.H.F., Castano, S., Dayal, U., Casati, F., de Oliveira, J.P.M. (eds) Conceptual Modeling - ER 2009. ER 2009. Lecture Notes in Computer Science, vol 5829. Springer, Berlin, Heidelberg.

ENDUROSAT X-Band 2x2 Patch Array Antenna | Satsearch. n.d. Satsearch.co. Accessed July 9, 2023. https://satsearch.co/products/endurosat-x-band-2x2-patch-array-antenna. 2023a

ENDUROSAT Onboard Computer with GNSS.” n.d. CubeSat by EnduroSat. https://www.endurosat.com/cubesat-store/cubesat-obc/onboard-computer-gnss/. 2023b

EXA Cubesat High Energy Density Battery | CubeSat.Market. n.d. Cubesat Market. https://www.cubesat.market/ba01-battery-array. 2023.

GENTINA, J. A Proposal for ITASAT Satellite Configuration and Its Preliminary Mission Analysis. 2009.

GOMES, B. et al. The Ground Segment Engineering Process for SPORT CubeSat Mission Operation. 2021

ISIS ANTENNA System for 6U/12U CubeSats | Satsearch. n.d. Satsearch.co. Accessed July 9, 2023. https://satsearch.co/products/isis-antenna-system-for-6u-12u-cube-sats.

KEPKAR, A. et al. Occurrence climatology of equatorial plasma bubbles derived using FormoSat-3 ⁄ COSMIC GPS radio occultation data. Annales Geophysicae, v. 38, n. 3, p. 611–623, 13 May 2020.

KILIC, C. et al. Deployment strategy study of QB50 network of CubeSats. 1 June 2013.

LARSON, W. J. Space mission analysis and design. Torrance, Calif.: Microcosm, 1997.

MORAES, A. DE O. et al. GPS availability and positioning issues when the signal paths are aligned with ionospheric plasma bubbles. GPS Solutions, v. 22, n. 4, 11 Jul. 2018.

ORDUY, J. et al. Pico And Nanosatellite Ground Station Architecture Development Reference Process. 2016.

SIDOROVA, L. N. Equatorial Plasma Bubbles: Variability of the Latitudinal Distribution with Altitude. Geomagnetism and Aeronomy, v. 61, n. 4, p. 508–519, Jul. 2021.

TAKAHASHI, H. et al. Equatorial plasma bubble seeding by MSTIDs in the ionosphere. Progress in Earth and Planetary Science, v. 5, n. 1, 11 Jun. 2018.

TENSOR TECH ADCS-MTQ Integrated Attitude Determination and Control System with Magnetorquers | Satsearch. n.d. Satsearch.co. Accessed July 9, 2023. https://satsearch.co/products/tensortech-adcs-mtq-integrated-attitude-determination-and-control-system-with-magnetorquers. 2023a.

TENSOR TECH RS100 - Tensor Tech | Reaction Wheel. Satnow.com. https://www.satnow.com/products/reaction-wheels/tensor-tech/38-1207-rs100. 2023b.

TSIOLKOVSKY, K. E. Investigation of outer space by reaction devices. Aeronautical Courier, 1911.

UMPPT Solar Panel Adder. n.d. Cubesat Market. https://www.cubesat.market/umppt. 2023.

VOIRIN, J.-L.; EXERTIER, D. Model-based System and Architecture Engineering with the Arcadia Method. [s.l.] Iste Press - Elsevier, 2017.

VRIES, D.; WIM. Cubesat Drag Calculations. Available at: https://www.osti.gov/biblio/1124870/.

YUE, X. et al. Space Weather Observations by GNSS Radio Occultation: From FORMOSAT-3/COSMIC to FORMOSAT-7/COSMIC-2. Space Weather, v. 12, n. 11, p. 616–621, Nov. 2014.

WOODRUFF, C. et al. Fiber-Fed Pulsed Plasma Thruster (FPPT) with Multi-Axis Thrust Vectoring. https://cuaerospace.com/Portals/0/SiteContent/assets/PDF/FPPT-IEPC22-Paper-v10-reduced.pdf. 2022.

ZOU, X. Global positioning system radio occultation observations. Atmospheric Satellite Observations, p. 175–205, 2020.

7. RESPONSIBILITY NOTICE

The authors are the only responsible for the printed material included in this paper.